

Random packing of small blocks: pressure effects, orientational correlations and application to polymer-based composites

Danilo Sergi, Claudio D'Angelo, Giulio Scocchi, and Alberto Ortona

University of Applied Sciences (SUPSI), The iCIMS Research Institute, Galleria 2, CH-6928 Manno, Switzerland

(Dated: September 7, 2021)

Packing is a complex phenomenon of prominence in many natural and industrial processes (liquid crystals, granular materials, infiltration, melting, flow, sintering, segregation, sedimentation, compaction, etc.). A variety of computational methods is available in particular for spheroid particles. Our aim is to apply the principle of the random sequential addition algorithm but with small blocks of varying size and orientation. Here the main purpose is to reproduce the observed arrangement of graphitic assemblies in polymeric matrices. Random packing is improved by applying an external pressure implemented with a drifted diffusive motion of the fillers. Attention is also paid to the emergence of structural and orientational order. Interestingly, mixtures of fillers of irregular shapes can be dealt with efficiently using the proposed algorithm.

Keywords: random packing, random sequential addition, block particles, reinforced polymers

I. INTRODUCTION

In the present Article we are faced with the problem of realizing the densest packing with small blocks out of a bimodal size distribution. The motivation is to generate the arrangement of graphitic assemblies in polymeric matrices as obtained after compaction (see Fig. 1). In these materials, the graphitic phase can reach high volume fractions. It follows that the packing structures of these systems demand attention, especially when the electrical properties are under investigation, since the polymer is insulating [1, 2]. More generally, the polymeric matrix is enriched with a second dispersed phase in order to enhance a wide range of properties of the resulting composite material (mechanical, electrical and thermal) [3]. In the appearance, this kind of materials display quite disordered microstructures that nonetheless reveal attributes of key importance in several aspects [4]. At the extremes, random packing can be addressed with detailed, fully deterministic numerical methods like classical molecular dynamics [5, 6] or with fully random processes [7, 8]. In between, dynamic approaches allowing the particles to change their size [9–12] appear to be the most established. Typically, it arises that the shape of the fillers has a significant influence on the packing properties (see in particular Refs. [9, 13]). Unfortunately, the mathematical treatment of general morphologies is far from being trivial and for this reason most of the research has so far concentrated on ellipsoidal particles (spheres, oblates and prolates), and in a few exceptions on cubes [14–16] and others [17]. Our work is based on the random sequential addition (RSA) algorithm [7] with the possibility to use hard fillers of arbitrary shape, similarly to what reported in Refs. [18–20] for 2D, but with coarser discretization for efficiency concerns. In order to favor compaction, we introduce the effect of an external pressure via a biased diffusive motion of the fillers. In principle, blocks can pack very well because they have extended planar surfaces [9]. When they can be rotated, severe geometrical constraints are imposed in their neighborhood. For this reason, the structural properties of the final configurations are analyzed in detail by means of radial distribution functions. Furthermore, we work out a method to detect orientational correlations at a local level. Our results suggest that

orientational correlations have a range that can go beyond that of structural order.

II. RANDOM ADDITION STRATEGY

The domain to be filled with small, impenetrable blocks has all side lengths equal to 1 with periodic boundary conditions. We build the blocks from small spheres of radius r , for the reasons explained in Ref. [18]. The blocks are obtained as follows. A single sphere is first placed randomly in the domain with uniform distribution. This sphere is that with the smallest x , y and z coordinates composing the block (before rotation). The other spheres are added so as to be aligned along the three cartesian axes with their centers separated by the distance r . Let l_x , l_y and l_z be the side lengths of the block; for example, the length of the x side is $l_x = (n_x + 1)r$, where n_x is the number of spheres aligned along this direction. The size of the block is fixed randomly by choosing n_x , n_y and n_z from three Gauss

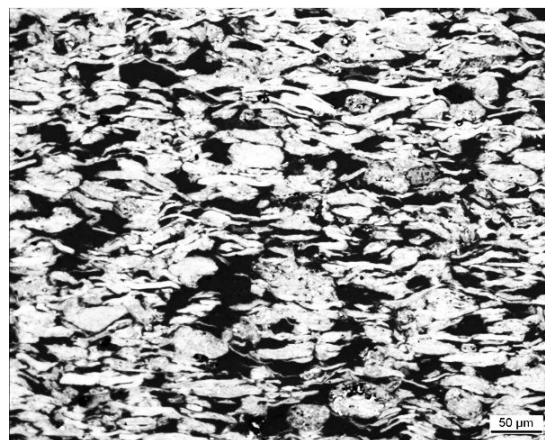


Figure 1: Microstructure geometry of a typical polymeric matrix reinforced with a graphitic powder. It appears that the graphitic phase (lighter) displays to a certain extent rectangular characteristics. By 2D image processing it is determined a volume fraction of around 62%.

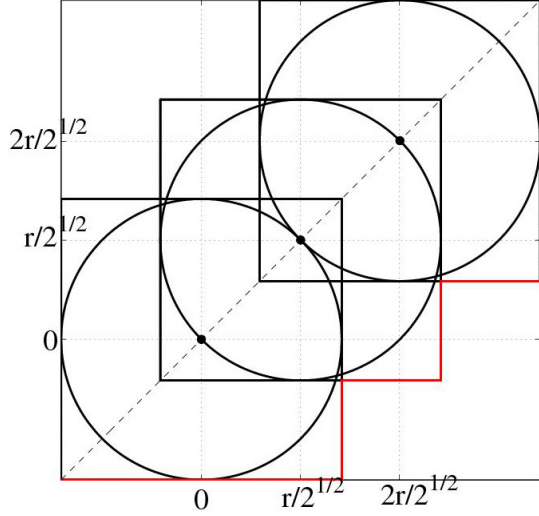


Figure 2: How the spheres are inscribed in the cubes. The origin of axes is in the center of the first placed sphere of the block. In red is shown the boundary of the block in the xy plane in the absence of tilt.

distributions of means $\langle n_x \rangle = (\langle l_x \rangle - r)/r$, $\langle n_y \rangle$ and $\langle n_z \rangle$; the three distributions have the same variance σ^2 and subsequent computations are done using the integer parts of n_x , n_y and n_z . The resulting block is then rotated around the z , x and y axes, in this order, by the angles θ_z , θ_x and θ_y , respectively. These three angles of rotation are chosen randomly within a given interval from a uniform distribution. For the rotation, the axes are translated with their origin in the center of the first sphere.

Let Δx , Δy and Δz be the distances in absolute value along the three axes between the centers of two spheres. This means that the two centers are separated by $\sqrt{(\Delta x)^2 + (\Delta y)^2 + (\Delta z)^2}$. The block is added to the domain if for every center of its spheres at least one Δ is larger than $2r + d_{\min}$ [21]. If this condition is not fulfilled there is overlap: the block is discarded and the above procedure is repeated.

We want to verify relatively fast the overlap condition. To this end, the domain is divided into five layers of equal width parallel to the xy plane. The centers of the spheres are stored in five lists, one for every layer. In order to avoid overlap at the interfaces, the spheres falling within a distance of $2r$ from an interface are also added to the list of the adjacent layer. In this way, the overlap condition is checked only among spheres belonging to the same list.

The binning of the domain is regular, leading to N^3 voxels. Every side of the domain is thus divided into N bins. Knowing the centers of the spheres, the real blocks are readily obtained at the end of the simulation by inscribing every sphere in a cube of side length $2r$. Every voxel inside the cubes will be considered as occupied by the filler phase. Voxels outside the cube will be considered instead as occupied by the matrix phase. By this procedure, the surface of the resulting parallelepipeds is rough. The degree of roughness is arguably in line with experimental observations. Indeed, we find that the depth of the defects is given approximately by the for-

mula $r |\cos \theta_z \sin \theta_z|$. The roughness is of course maximal for $\theta_z = \pi/4$. By simple geometrical arguments, we find that the depth of the incidents at the surface is approximately at most $r/2$ (see Fig. 2). This value corresponds to 1% of the side of the simulation domain for $r = 0.02$. Indicatively, the side of the simulation domain can be assumed to be 350 μm , leading to a depth of the defects of the surface of 3.5 μm . In the case of graphite-polymer composites, we observe that at the micron scale the surface of the fillers is irregular (see Fig. 1).

Diffusive motion is introduced by means of random moves of the blocks along the x , y and z directions. The effect of an external pressure is accounted for by introducing a bias toward the center of the domain. More precisely, after a given number of unsuccessful attempts, all the already placed blocks are moved randomly. For every block, first the direction of the trial move is chosen randomly. The sense of the move is then chosen with probabilities p_x , p_y and p_z . For example, for a block with the first sphere in the region defined by $x > 1/2$, p_x is the probability to be translated toward the center with sense and direction defined by the vector $(-1, 0, 0)$. Given a block, the distance spanned by the trial moves is different for every direction. When a move is not possible because resulting in overlap, the distance associated with that direction is reduced by a factor of 2. The first time one of the possible move distances falls below d_{\min} , the block is no more taken into account for random moves. Finally, in this way, purely diffusive motion corresponds to $p_x = p_y = p_z = 0.5$ while in all other cases there appears a resultant pressure (inward or outward oriented).

III. SIMULATION SETTINGS AND MODELING APPROACH

In all simulations reported here, the standard deviation σ is set to the value $\sqrt{0.3}$ and the radius of the spheres is $r = 0.02$. We always start with a given average size and smaller blocks are considered when no block can be placed after 200'000 trials. The simulation is terminated when no smaller block can be placed for the same condition. Table I lists the powders with the average size of blocks they are composed of. Mixtures and aspect ratios are chosen so as to obtain composite materials produced experimentally by using common graphitic powders.

Different random orientations are investigated. We distinguish the types of arrangement listed in Tab. II. Every system is considered without diffusion and pressure and with pressure. In the latter case, for the probabilities of rearrangement we choose $p_x = p_y = p_z = 1$ in order to reach the maximal packing fractions. The initial possible displacement along the three directions is 0.5. The minimal distance of approach is set to $d_{\min} = 2/N$, with $N = 256$, corresponding to the width of two adjacent voxels. The blocks are never moved twice consecutively, but one unsuccessful attempt is sufficient in order to call the routine performing diffusive motion. The aim is to keep the pressure effect as close as possible to the linear dependence on the total number of blocks when present in

	Particle1	Particle2	Volume ratio
bimodal1	(0.2, 0.2, 0.12)	(0.06, 0.06, 0.04)	33.3 : 1
bimodal2	(0.2, 0.2, 0.12)	(0.1, 0.1, 0.06)	8 : 1
bimodal3	(0.2, 0.2, 0.12)	(0.14, 0.14, 0.08)	3.1 : 1
granular	(0.2, 0.2, 0.12)	(0.2, 0.2, 0.12)	1 : 1
fine	(0.06, 0.06, 0.04)	(0.06, 0.06, 0.04)	1 : 1

Table I: Generated powders of different mixtures. The vectors (l_x, l_y, l_z) defines the average side lengths of the blocks.

No.	Type	θ_x	θ_y	θ_z
I	aligned	0	0	0
II	misaligned	0	0	$[-\pi/4, +\pi/4]$
III	tilted x	$[-\pi/36, +\pi/36]$	0	0
IV	tilted xy	$[-\pi/36, +\pi/36]$	$[-\pi/36, +\pi/36]$	0
V	misaligned and tilted x	$[-\pi/36, +\pi/36]$	0	$[-\pi/4, +\pi/4]$
VI	misaligned and tilted xy	$[-\pi/36, +\pi/36]$	$[-\pi/36, +\pi/36]$	$[-\pi/4, +\pi/4]$

Table II: Case studies and their orientation characteristics.

	I	II	III	IV	V	VI
bimodal1 (std)	55.1%	49.5%	54.4%	52.5%	50.1%	49.4%
bimodal1 (press)	59.5%	54.3%	57.4%	57.2%	54.9%	52.1%
bimodal2 (std)	52.0%	49.3%	52.2%	51.0%	47.2%	47.9%
bimodal2 (press)	58.7%	51.4%	56.7%	55.7%	51.0%	50.3%
bimodal3 (std)	50.4%	45.0%	48.8%	48.8%	43.1%	42.9%
bimodal3 (press)	54.9%	47.6%	52.9%	51.5%	46.1%	46.5%
granular (std)	40.9%	37.0%	38.8%	41.5%	35.7%	34.7%
granular (press)	44.5%	40.3%	43.0%	41.3%	42.4%	37.9%
fine (std)	34.1%	33.4%	33.8%	33.8%	32.8%	33.3%
fine (press)	36.6%	35.7%	36.4%	36.3%	35.8%	35.7%

Table III: Packing fractions as obtained from simulations for systems with different orientational characteristics and size distributions. The name of the mixtures is defined in Tab. I. The labels I-VI refer to the systems with the degree of orientational randomness defined in Tab. II. The abbreviation std stands for standard (without pressure and diffusive motion); press means that an external pressure is applied as explained in Sec. III.

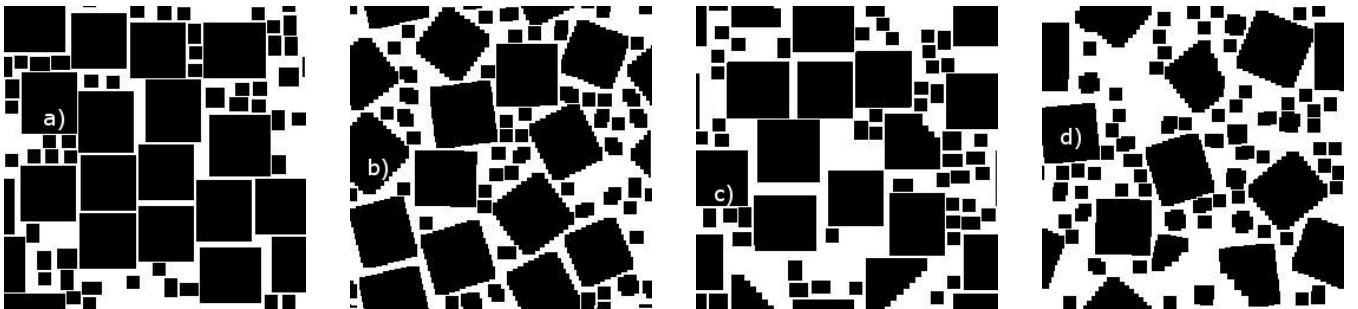


Figure 3: Sections of some packing structures for the mixture bimodal1 (see Tab. I) with an applied external pressure. a) Aligned case. b) Misaligned case. c) Tilted xy case. Note that the boundary of the blocks in the plane xy can be diagonal. d) Misaligned and tilted xy case. Note that the boundary of the blocks can be irregular in this case.

		I		II		III		IV		V		VI	
		no. part.	density	no. part.	density	no. part.	density	no. part.	density	no. part.	density	no. part.	density
bimodal1 (std)	large	101	41.8%	81	34.2%	93	40.1%	91	37.9%	81	35.0%	77	34.2%
	small	1'222	13.3%	1'423	15.3%	1'325	14.3%	1'345	14.6%	1'436	15.1%	1'448	15.2%
bimodal1 (press)	large	110	45.4%	88	38.9%	100	41.8%	102	42.9%	92	41.1%	81	35.9%
	small	1'263	14.1%	1'405	15.4%	1'415	15.6%	1'290	14.3%	1'271	13.8%	1'498	16.2%
bimodal2 (std)	large	93	38.1%	85	36.7%	90	37.7%	90	37.4%	81	34.6%	83	36.0%
	small	346	13.9%	310	12.6%	368	14.5%	335	13.6%	288	12.6%	292	11.9%
bimodal2 (press)	large	110	45.7%	88	38.5%	103	43.4%	100	43.2%	91	40.0%	88	38.9%
	small	325	13.0%	310	12.9%	334	13.3%	299	12.5%	265	11.0%	275	11.4%
bimodal3 (std)	large	98	41.1%	85	36.9%	88	37.7%	89	37.9%	81	35.9%	76	33.7%
	small	80	9.3%	65	8.1%	96	11.1%	93	10.9%	57	7.2%	73	9.2%
bimodal3 (press)	large	104	43.5%	89	38.6%	98	42.1%	103	44.1%	92	40.2%	84	38.3%
	small	98	11.4%	71	9.0%	92	10.8%	61	7.4%	47	5.9%	66	8.2%
granular (std)	large	99	40.9%	88	37.0%	92	38.8%	98	41.5%	81	35.7%	80	34.7%
	small	0	0%	0	0%	0	0%	0	0%	0	0%	0	0%
granular (press)	large	107	44.5%	93	40.3%	104	43.0%	98	41.3%	90	42.4%	86	37.9%
	small	0	0%	0	0%	0	0%	0	0%	0	0%	0	0%
fine (std)	large	0	0%	0	0%	0	0%	0	0%	0	0%	0	0%
	small	3'066	34.1%	3'000	33.4%	3'014	33.8%	3'063	33.8%	2'962	32.8%	2'993	33.3%
fine (press)	large	0	0%	0	0%	0	0%	0	0%	0	0%	0	0%
	small	3'231	36.6%	3'148	35.7%	3'182	36.4%	3'191	36.3%	3'144	35.8%	3'138	35.7%

Table IV: Number of block particles of type larger and smaller composing every bimodal powder and their contribution to the packing density. Misalignment of larger blocks is the primary cause of significant variations of the overall volume fraction. The mixtures and the size of their particles are introduced in Tab. I. Roman numbers specify the degree of orientational randomness as defined in Tab. II.

relatively large number.

Of course, the application of an external load has the effect to deform the fillers. Furthermore, anisotropic pressures can also lead to a certain degree of orientational order. We apply an isotropic pressure, but the shape of the fillers and the restricted range of the tilt angles intend to simulate the effect of uniaxial compaction along the z direction. Graphitic powders are the result of an extremely expensive process of milling. Because of their molecular structure, the size of particles is reduced through both exfoliation and fragmentation. It is clear that the combination of these phenomena introduces faces and angularities in the resulting particles. In that respect, the block is the simplest geometry approaching the shape of real graphitic assemblies.

IV. RESULTS AND DISCUSSION

In Tab. III, the packing fractions ϕ reached for the different powders and orientational characteristics are reported. In general, the application of pressure leads to denser packings. We ascribe the unique exception to statistical fluctuations. Indeed, for the granular powder of type IV with pressure, average over five realizations gives $\phi = 0.422$, in this case above the value for the same system with no applied pressure. For comparative purposes relative to the different orientational properties,



Figure 4: 3D rendering of the final structure for the powder bimodal2 with pressure in the aligned case. The volume fraction is 58.7%.

Fig. 3 shows the sections of four final configurations for the powder bimodal1 with an applied pressure. In this case, the highest packing values are reached since the smaller particles can better fill the irregular interstices between larger blocks.

	I	II	III	IV	V	VI
bimodal1 (std)	0-0	0.5159-0.1329	0-0	0-0	0.5209-0.1355	0.5072-0.1287
	0-0	0-0	0.0586-0.0017	0.0588-0.0017	0.0585-0.0017	0.0590-0.0017
	0-0	0-0	0-0	0.0576-0.0017	0-0	0.0585-0.0017
bimodal1 (press)	0-0	0.5140-0.1321	0-0	0-0	0.5142-0.1324	0.5084-0.1294
	0-0	0-0	0.0579-0.0017	0.0577-0.0017	0.0570-0.0016	0.0585-0.0017
	0-0	0-0	0-0	0.0581-0.0017	0-0	0.0580-0.0017
bimodal2 (std)	0-0	0.4895-0.1206	0-0	0-0	0.4761-0.1153	0.4808-0.1182
	0-0	0-0	0.0571-0.0016	0.0565-0.0016	0.0550-0.0015	0.0564-0.0016
	0-0	0-0	0-0	0.0553-0.0015	0-0	0.0566-0.0016
bimodal2 (press)	0-0	0.4780-0.1146	0-0	0-0	0.4884-0.1198	0.4935-0.1218
	0-0	0-0	0.0584-0.0017	0.0586-0.0017	0.0553-0.0015	0.0553-0.0015
	0-0	0-0	0-0	0.0585-0.0017	0-0	0.0565-0.0016
bimodal3 (std)	0-0	0.5001-0.1248	0-0	0-0	0.4896-0.1227	0.4707-0.1114
	0-0	0-0	0.0579-0.0017	0.0533-0.0014	0.0493-0.0012	0.0568-0.0016
	0-0	0-0	0-0	0.0570-0.0016	0-0	0.0583-0.0017
bimodal3 (press)	0-0	0.4870-0.1186	0-0	0-0	0.4694-0.1127	0.4577-0.1077
	0-0	0-0	0.0545-0.0015	0.0566-0.0016	0.0538-0.0016	0.0590-0.0017
	0-0	0-0	0-0	0.0524-0.0014	0-0	0.0556-0.0015
granular (std)	0-0	0.4949-0.1200	0-0	0-0	0.4870-0.1222	0.4779-0.1185
	0-0	0-0	0.0555-0.0015	0.0571-0.0016	0.0531-0.0014	0.0532-0.0014
	0-0	0-0	0-0	0.0548-0.0015	0-0	0.0579-0.0016
granular (press)	0-0	0.5175-0.1336	0-0	0-0	0.4617-0.1126	0.5162-0.1312
	0-0	0-0	0.0579-0.0016	0.0537-0.0014	0.0609-0.0018	0.0601-0.0018
	0-0	0-0	0-0	0.0577-0.0016	0-0	0.0570-0.0016
fine (std)	0-0	0.5227-0.1366	0-0	0-0	0.5162-0.1332	0.5146-0.1325
	0-0	0-0	0.0589-0.0017	0.0581-0.0017	0.0581-0.0017	0.0581-0.0017
	0-0	0-0	0-0	0.0582-0.0017	0-0	0.0576-0.0017
fine (press)	0-0	0.5200-0.1351	0-0	0-0	0.5162-0.1331	0.5095-0.1299
	0-0	0-0	0.0589-0.0017	0.0581-0.0017	0.0578-0.0017	0.0587-0.0017
	0-0	0-0	0-0	0.0574-0.0016	0-0	0.0587-0.0017

Table V: Average value and variance of the variables $\Delta\theta$ for the case studies of Tabs. I and II. For every mixture, the first row refers to $\Delta\theta_z$ followed by its variance, the second to $\Delta\theta_x$ and its variance, and the third to $\Delta\theta_y$ and its variance. The abbreviations std and press mean with no pressure and with pressure, respectively.

Figure 4 shows the 3D representation of the packing structure when the role of pressure is more effective (bimodal2 powder of type I). In general, orientational disorder lowers the packing density in particular if misalignment is allowed (see Fig. 5). Fine powders lead to looser random packings. It turns out that the highest volume fractions can be achieved with more polydisperse size distributions by starting from the addition of larger blocks in the absence of orientational disorder. The role of smaller particles is to fill progressively narrower interstices. In this way, it is possible to simulate the infiltration of finer powders between stuck particles and eventually their aggregation. Table IV further details the results for the packing structures of all powders.

It is interesting to look at how the packing fraction progresses in the course of time. Figure 6 shows the cases of

granular and fine powders of type I (aligned case). With pressure, the volume fraction follows a power law $\phi \sim t^\gamma$ over one more decade. Furthermore, at the end, these simulations are faster. For other orientational characteristics, it is found that ϕ displays an analogous behavior. In the case of bimodal powders, we also find similar curves for the addition of smaller blocks.

In order to gain insight into the structural properties of the final configurations of the generated powders, we calculate the radial distribution functions (RDFs) between types of blocks. The usual definition of the RDF $g(r)$ is [22]

$$\frac{N_1}{V} g(r) 4\pi r^2 \Delta r = S(r) . \quad (1)$$

$V = 1$ is the volume of the domain. $S(r)$ is the average number of particles of type 2 falling within a spherical shell of radius

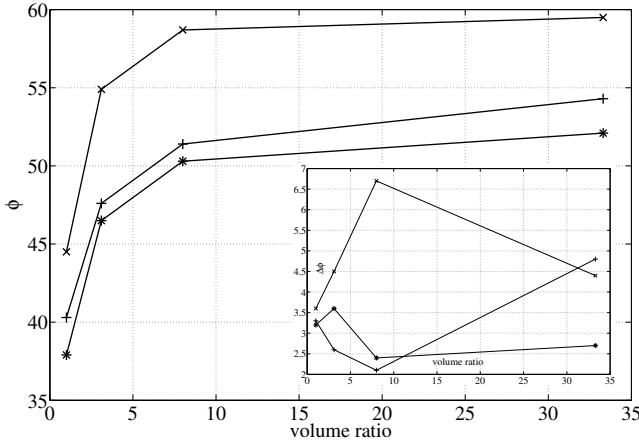


Figure 5: Packing fraction against the volume ratio; pressure is applied. Aligned case (×), misaligned case (+) and misaligned with tilt xy case (*) (cf. Fig. 3). Inset: $\Delta\phi = \phi_{\text{press}} - \phi_{\text{std}}$ as a function of the volume ratio. ϕ_{press} is the packing fraction reached with pressure and ϕ_{std} that realized with no pressure.

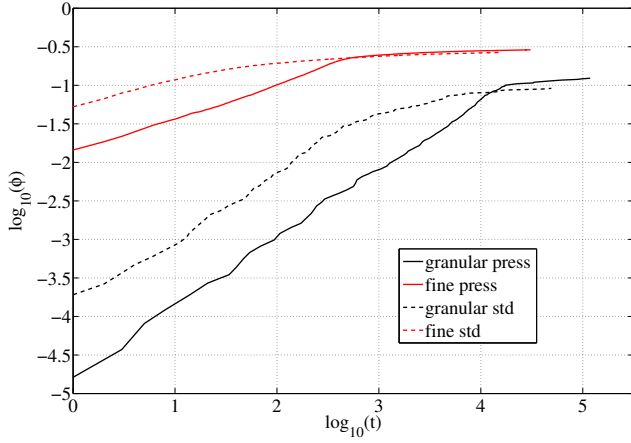


Figure 6: Packing fraction ϕ as a function of time (log-log scale). All powders are of type aligned (cf. Tab. II) with pressure (press) and with no pressure (std).

r and width Δr centered around the particles of type 1 present in number N_1 . (Precisely, the distance between two blocks is determined using their centers of mass.) As a consequence, the RDF is a measure of the average radial dependence of the density of particles of type 2 around those of type 1. In the following, given a powder, with the notation $g_{1s}(r)$ we intend the RDF of smaller particles around larger ones. We employ similar notations for the other cases and, with no upper-script, the RDF is among all particles. Figure 7 shows different RDFs in several cases. In the first row, the main peak of g_{11} is determined by adjacent in-plane blocks. The first peak around $r = 0.1$ is due to the elongated shape of the blocks. It is lower than the second peak because a block can have indicatively twice more in-plane neighbors. In the absence of pressure (second row), it is seen that the peaks are lower and slightly broader, indicating that these structures are less compact. Of course, these remarks hold also for the other bimodal pow-

ders. The third row of Fig. 7 shows g_{1s} for different mixtures. Mainly, as the volume ratio gets smaller, there appears more distinctly a peak at $r \approx 0.1$. This means that the contribution of out-of-plane small particles become statistically more significant. For the powder bimodal3, the last peak around $r = 0.4$ is related to the first peak of g_{11} and corresponds to pairs of large-small blocks separated by a large one. For the bimodal1 powder, the first peak of g_{ss} always occurs before $r = 0.1$ (fourth row). It follows that this peak is due to the small particles filling the voids between larger blocks. The same RDF for the fine powder is similar (fifth row). The absence of interstices between larger blocks has no consequence because the small particles tend to fill densely the voids. Indeed, for the other bimodal powders there appear additional peaks after $r = 0.1$, more distinctly for the lowest volume ratio (bimodal3 powder). The RDF among all particles for the bimodal1 powder (last row) tells us that the statistics is dominated by the small particles relatively close to each other determining the first peak. In the other cases, the arrangement of smaller blocks is progressively similar to that of larger ones and there appear two peaks for $r \geq 0.1$ for the reasons explained above (see first row).

Interestingly, Fig. 3 suggests that the orientation of larger blocks might be correlated. In order to better understand this point, we carry out a statistics of the rotation angles. Let P be the number of possible pairs of blocks. We introduce the average quantities

$$\langle \Delta\theta_z \rangle = \frac{1}{P} \sum_{i>j}^P |\theta_z(i) - \theta_z(j)|;$$

$$\langle (\Delta\theta_z)^2 \rangle = \frac{1}{P} \sum_{i>j}^P [\theta_z(i) - \theta_z(j)]^2.$$

$\theta_z(i)$ is the rotation angle of the i -th block. Similar average values are defined for the tilt angles θ_x and θ_y . Besides the average values $\langle \Delta\theta \rangle$, of interest are also the variances $\langle (\Delta\theta)^2 \rangle - \langle \Delta\theta \rangle^2$. In Tab. V these quantities are given in all cases addressed by simulations. The blocks are expected to have the same orientation to a higher degree when the quantities $\langle \Delta\theta \rangle$ are small. It is important to remark that $\langle \Delta\theta_z \rangle$ can be at most $\pi/2$. It is found that this quantity varies in the interval $0.4617 - 0.5227$, i.e. $26^\circ - 30^\circ$. As a result, from this overall statistics it clearly arises that orientational ordering is present in the internal packing structures. However, it seems difficult to discriminate between and compare the different cases on the basis of this method.

The emergence of orientational order can be addressed in a more specific way. Let B be the number of blocks. We define $B_i(r)$ as the ensemble of blocks inside a spherical shell of radius r and width Δr centered around the i -th block. In order to take into account the local, relative orientation of pairs of blocks, we introduce the function

$$S_z(r) = \sum_i^B \sum_{j \in B_i(r)} \frac{(\Gamma/2)^2}{[\theta_z(i) - \theta_z(j)]^2 + (\Gamma/2)^2}.$$

$\theta_z(i)$ is the angle of rotation around the z axis of the i -th block; the constant Γ is assumed to be 10^{-4} . In the above

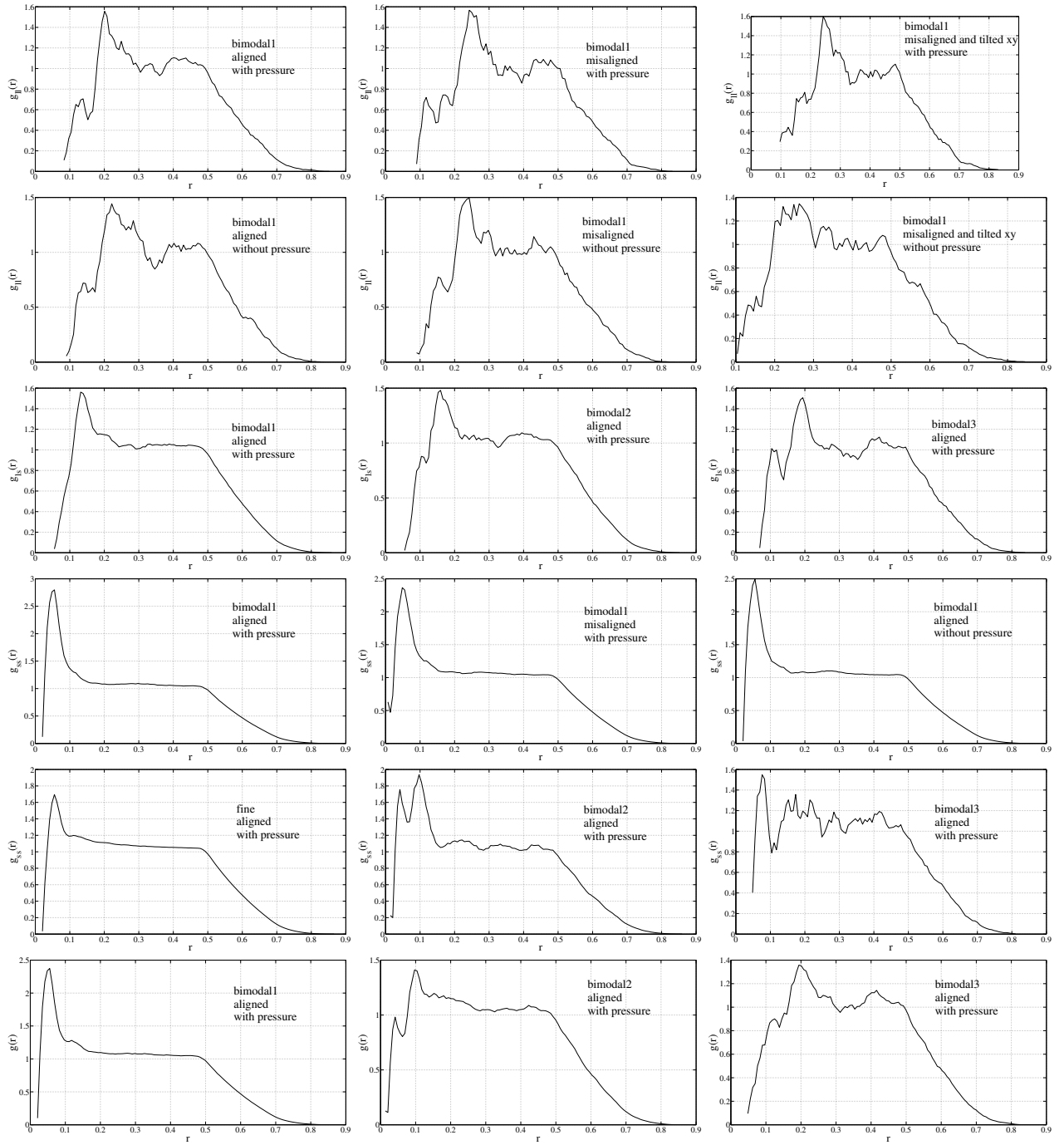


Figure 7: Representative RDFs. For Δr we choose 5/256 (see Eq. 1).

sum, the idea is that the contribution of every pair of block is "weighted" by a Lorentz function. Summands close to 1 indicate that the corresponding θ_z angles of the blocks differ slightly. Substitution into Eq. 1 yields a kind of RDF $g_z(r)$ measuring the average radial dependence of orientational correlations. Similar definitions hold for the functions g_x and g_y . For completeness, we also consider the function g_u defined by using the angle formed by the orientation vectors of pairs of blocks. For every block, the orientation vector is initially

$\mathbf{u} = (1, 0, 0)$, to which three rotation transformations of angles θ_z , θ_x and θ_y are applied in this order. In Fig. 8, we plot these functions for two powders in different cases of orientational randomness. For the functions g_z of the bimodal1 powder (first row), the peaks around $r = 0.3$ indicate that the orientation of every block is to a certain degree correlated with that of its adjacent blocks. From the further peaks we can conclude that the orientation is also correlated between second-nearest neighbors (see Fig. 3). For the functions g_x and g_y (second

	bimodal1	bimodal2	bimodal3	granular	fine
no pressure	57.9%	53.2%	48.3%	38.5%	37.9%
with pressure	59.8%	54.8%	50.3%	41.6%	42.0%

Table VI: Packing fractions reached for powders composed of spherical particles. The average diameters of the two types of spheres are equal to the longest side of the blocks for the corresponding mixture of Tab. I. Since simulations are much faster in this case, smaller spheres are considered after 2×10^6 unsuccessful attempts; all other simulation settings are maintained.

row), the average values are always at least a factor 20 larger than for the previous g_z functions. The reason is that the tilt angles are restricted to values belonging to small intervals. The presence of more peaks is consistent with the elongated shape of particles. For g_x all peaks are comparable in height; instead, for g_y there appears a marked peak around $r = 0.3$. Without pressure (third row), the peaks are reduced in height and that near $r = 0.3$ is always the more pronounced. This means that orientational correlations among second-nearest neighbors are weaker because of looser packing. For the bimodal3 powder (fourth and fifth rows), from the peaks in the range $r = 0.1 - 0.2$ it turns out that out-of-plane blocks are also correlated. This peak is of course higher for the functions g_x and g_y . Furthermore, in this case the functions g_x and g_y under the same conditions are similar (see second row). In the last row, the function g_u is considered for three different powders. Direct comparison with the plots of the functions g_x , g_y and g_z for the same type of powders indicate that the first peaks flatten out. It follows that, for adjacent in-plane blocks, the angles θ_x are weakly correlated; for out-of-plane blocks, it arises that the angles θ_z are instead weakly correlated.

We end this section by pointing out that every simulation used around 20 MB of RAM memory and the longest run took 74h 43min (bimodal3 powder aligned case with pressure) while the shortest one lasted for 3h 51min (fine powder tilted x case without pressure). The program is written in Perl and it is executed on a desktop computer with an Intel processor of the family i7. Finally, Tab. VI provides the packing fractions achieved with equivalent spherical fillers. These results are comparable with the predictions for random packing of spheres [11, 23–26], indicating that volume fractions can reach values in the interval 0.60–0.68. It arises that the role of pressure is more effective with coarse blocks. The best volume fractions can not be reached within the present simulation settings because we can not tune arbitrarily parameters like the aspect ratios, the relative size between small and large blocks and between the particles and the simulation domain, given the specific application under investigation. It clearly turns out that higher volume fractions can be realized only with more polydispersity.

V. CONCLUSIONS

It is well-known that the shape and size of the fillers affect the packing outcome and in turn, for example, the accurate prediction of the properties of materials by finite element methods [27]. In this work we focused on small blocks because they better approximate the shape of graphitic clusters in some aspects (edges and corners). The algorithm is based on random sequential addition and can be extended easily to fillers with more irregular shapes, domains with solid walls or random addition mimicking deposition. In this approach, the interaction and evolution of the relevant constituents of the material are poorly accounted for. The main advantage of stochastic methods is the possibility to treat efficiently the complexity of the systems by concentrating on simple, effective rules [28]. In the case of the present algorithm, full control on interparticle distance seems to be the most useful property when the potential energy between hard particles is assumed to be identically zero, except for the case of contact. Then, coarser discretization clearly expedites the simulations. Unavoidably, this leads to defects at the surfaces, but roughness is a ubiquitous element in materials science. In the case of bimodal packing our results show that more polydisperse size distributions could lead to higher volume fractions, because particles are more suited to fill voids comparable to their size. In any case, bimodal size distributions deserve attention for the transport properties associated with their particular packing structures. Radial distribution functions provides useful information on the size, amount and arrangement of the particles composing the systems. Our analysis on correlations reveals that structural and orientational order do not coincide. It turns out that a nonstructured medium (beyond the radial distance $r = 0.3$ in our systems) can still display forms of organization.

VI. NOMENCLATURE

A. Symbols

B	-	number of block particles in the simulation domain
B_i	-	number of blocks in a spherical shell of radius r centered around the i -th block
d_{\min}	-	minimal distance of approach between two block particles
$g_{ll}, g_{ls}, g_{ss}, g$	-	radial distribution functions
g_x, g_y, g_z, g_u	-	functions defined for detecting orientational order
l_x, l_y, l_z	-	side length of block particles
N	-	number of voxels along each side of the simulation domain
N_1	-	number of block particles of type 1
n_x, n_y, n_z	-	number of spheres composing each side of block particles

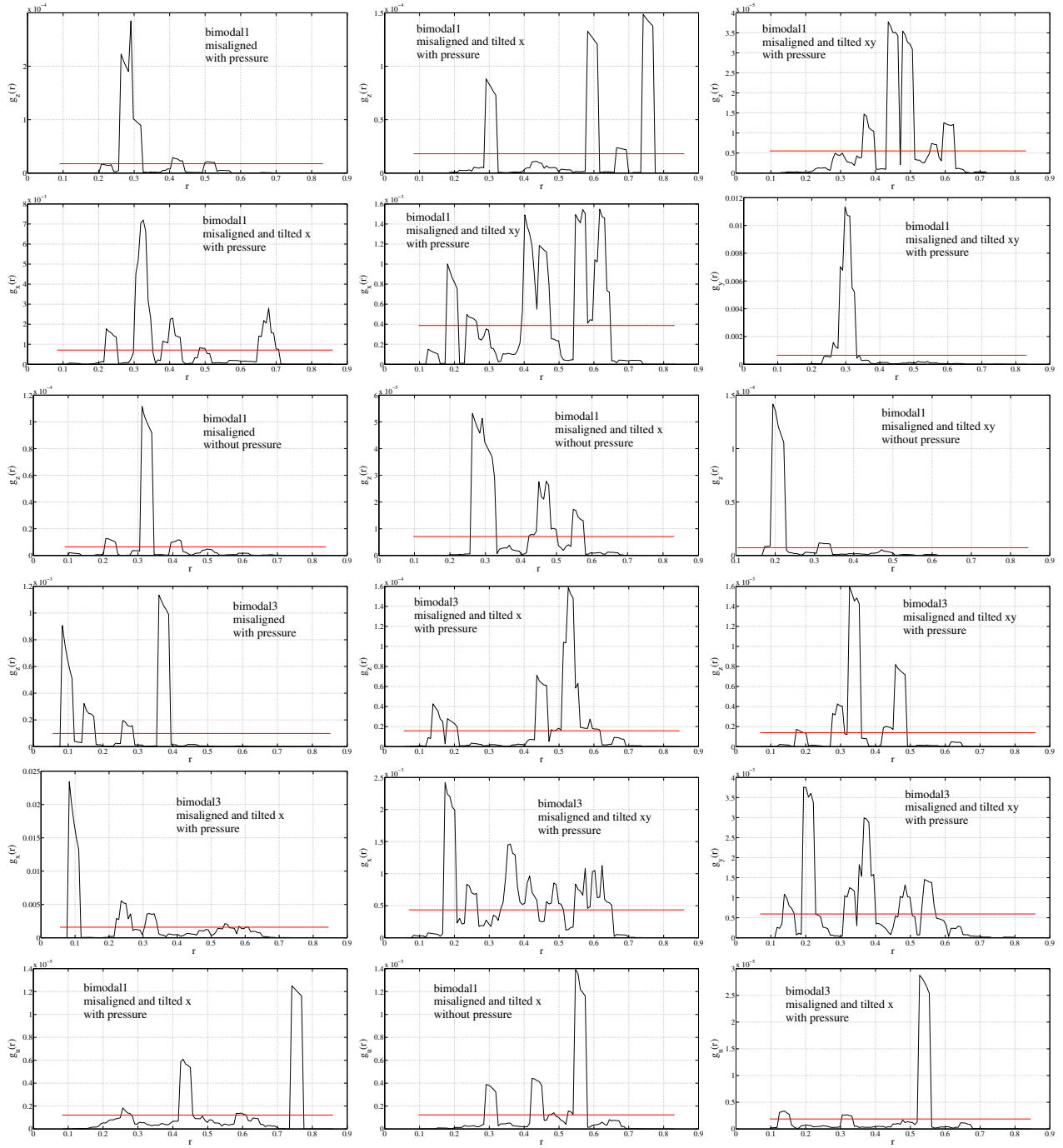


Figure 8: Functions g_x , g_y , g_z and g_u for the mixtures bimodal1 and bimodal3 (cf. Tab. I) for different orientational characteristics (see Tab. II). Δr is set to $5/256$ (cf. Eq. 1). For the powder bimodal1, small particles are omitted. The straight line in red shows the average value. It is calculated by averaging the functions over the bins.

P	- number of pairs of blocks in the simulation domain	S_x, S_y, S_z, S_u	- weighted number of block particles in a spherical shell of radius r
p_x, p_y, p_z	- probability for random moves along each axis	t	- time
r	- radius of spheres composing block particles	\mathbf{u}	- unit vector
Δr	- width of a spherical shell	x, y, z	- cartesian coordinates
S	- average number of block particles in a spherical shell of radius r	V	- volume of simulation domain

Γ	-	model parameter	press	with pressure
γ	-	power-law exponent	RDF	radial distribution function
ϕ	-	volume fraction	RSA	random sequential addition
σ	-	standard deviation of a Gauss distribution	std	standard
$\theta_x, \theta_y, \theta_z$	-	rotation angles around each axis		

B. Abbreviations

min	minimum
part.	particles

Acknowledgments

This work was supported through project BiPCaNP (P. No. 10055.1) by the Swiss Commission for Technological Innovation (KTI/CTI).

-
- [1] G. Ambrosetti, N. Johner, C. Grimaldi, A. Danani, P. Ryser, Percolative properties of hard oblate ellipsoids of revolution with a soft shell, *Phys. Rev. E* **2008**, *78*, 61126-61136.
- [2] G. Ambrosetti, C. Grimaldi, I. Balberg, T. Maeder, A. Danani, P. Ryser, Solution of the tunneling-percolation problem in the nanocomposite regime, *Phys. Rev. B* **2010**, *81*, 155434-155445.
- [3] M. Galli, J. Botsis, J. Janczak-Rusch, An elastoplastic three-dimensional homogenization model for particle reinforced composites, *Comput. Mat. Sci.* **2008**, *41*, 312-321.
- [4] S. Torquato, *Random Heterogeneous Materials: Microstructures and Macroscopic Properties*. Springer-Verlang, New York, **2002**.
- [5] R. Berardi, C. Fava, C. Zannoni, A Gay-Berne potential for dissimilar biaxial particles, *Chem. Phys. Lett.* **1998**, *297*, 8-14.
- [6] R. Everaers, M.R. Ejtehadi, Interaction potentials for soft and hard ellipsoids, *Phys. Rev. E* **2003**, *67*, 41710-41717.
- [7] B. Widom, Random sequential addition of hard spheres to a volume, *J. Chem. Phys.* **1966**, *44*, 3888-3894.
- [8] J.D. Sherwood, Packing of spheroids in three-dimensional space by random sequential addition, *J. Phys. A* **1997**, *30*, 839-843.
- [9] A. Donev, I. Cisse, D. Sachs, E.A. Variano, F.H. Stillinger, R. Connelly, S. Torquato, P.M. Chaikin, Improving the density of jammed disordered packings using ellipsoids, *Science* **2004**, *303*, 990-993.
- [10] B.D. Lubachevsky, F.H. Stillinger, Geometric properties of random disk packings, *J. Stat. Phys.* **1990**, *60*, 561-583.
- [11] W.S. Jodrey, E.M. Tory, Computer simulation of close random packing of equal spheres, *Phys. Rev. A* **1985**, *32*, 2347-2351.
- [12] A. Bezrukov, D. Stoyan, Simulation and statistical analysis of random packings of ellipsoids, *Part. Part. Syst. Charact.* **2006**, *23*, 388-398.
- [13] W. Man, A. Donev, F.H. Stillinger, M.T. Sullivan, W.B. Russel, D. Heeger, S. Inati, S. Torquato, P.M. Chaikin, Experiments on random packings of ellipsoids, *Phys. Rev. Lett.* **2005**, *94*, 198001-198004.
- [14] J.A. Elliott, A.H. Windle, A dissipative particle dynamics method for modeling the geometrical packing of filler particles in polymer composites, *J. Chem. Phys.* **2000**, *113*, 10367-10376.
- [15] A. Munjiza, J.-P. Latham, Comparison of experimental and numerical results for gravitational deposition of identical cubes, *Engng. Computat.* **2004**, *21*, 249-264.
- [16] L.-P. Lathan, A. Munjiza, The modelling of particle systems with real shapes, *Phil. Trans. R. Soc. Lond. A* **2004**, *362*, 1953-1972.
- [17] X. Jia, M. Gan, R.A. Williams, D. Rhodes, Validation of a digital packing algorithm in predicting powder packing densities, *Powder Technol.* **2007**, *174*, 10-13.
- [18] X. Jia, R.A. Williams, A packing algorithm for particles of arbitrary shapes, *Powder Technol.* **2001**, *120*, 175-186.
- [19] X. Jia, N. Gopinathan, R.A. Williams, Modeling complex packing structures and their thermal properties, *Adv. Powder Technol.* **2002**, *13*, 55-71.
- [20] R. Caulkin, X. Jia, M. Fairweather, R.A. Williams, Geometric aspects of particle segregation, *Phys. Rev. E* **2010**, *81*, 51302-51310.
- [21] This choice is tightly related to the way the blocks are obtained from the spheres (cf. next paragraph). The distance d_{\min} is introduced so that the blocks remain completely impenetrable, i.e., with no contact between their surfaces.
- [22] L.E. Reichl, *A Modern Course in Statistical Physics*. Wiley-VCH, Weinheim, **2009**.
- [23] S. Torquato, T.M. Truskett, P.G. Debenedetti, Is random close packing of spheres well defined?, *Phys. Rev. Lett.* **2000**, *84*, 2064-2067.
- [24] W.M. Wisscher, M. Bolsterli, Random packing of equal and unequal spheres in two and three dimensions, *Nature (London)* **1972**, *239*, 504-507.
- [25] J. Tobochnik, P.M. Chapin, Monte Carlo simulation of hard spheres near random closest packing using spherical boundary conditions, *J. Chem. Phys.* **1988**, *88*, 5824-5830.
- [26] S.R. Williams, A.P. Philipse, Random packings of spheres and spherocylinders simulated by mechanical contraction, *Phys. Rev. E* **2003**, *67*, 51301-51309.
- [27] R.B. Bohn, E.J. Garboczi, User manual for finite element and finite difference programs: A parallel version of NISTIR-6269, NIST Internal Report **2003**, 6997, 1-275.
- [28] N. Goldenfeld, L.P. Kadanoff, Simple lessons from complexity, *Science* **1999**, *284*, 87-89.